Zou et al. Molecular Cancer (2024) 23:205
https://doi.org/10.1186/s12943-024-02117-5

Molecular Cancer

RESEARCH Open Access

FTO-mediated DSP m^{6}A demethylation promotes an aggressive subtype of growth hormone-secreting pituitary neuroendocrine tumors

Yunzhi Zou[1†], Xiaoqiong Bao[1†], Depei Li[1†], Zhen Ye[2†], Rong Xiang[1], Yuanzhong Yang[1], Zhe Zhu[3], Ziming Chen[1], Lingxing Zeng[1], Chunling Xue[1], Hongzhe Zhao[1], Boyuan Yao[2], Qilin Zhang[2], Zeming Yan[1], Zekun Deng[1], Jintong Cheng[1], Guanghao Yue[1], Wanming Hu[1], Jixiang Zhao[1], Ruihong Bai[1], Zhenhua Zhang[4], Aiqun Liu[5*], Jialiang Zhang[1*], Zhixiang Zuo[1*] and Xiaobing Jiang[1*]

Abstract

Background Growth hormone-secreting pituitary neuroendocrine tumors can be pathologically classified into densely granulated (DGGH) and sparsely granulated types (SGGH). SGGH is more aggressive and associated with a poorer prognosis. While epigenetic regulation is vital in tumorigenesis and progression, the role of N^6-methyladenosine (m^{6}A) in aggressive behavior has yet to be elucidated.

Methods We performed m^{6}A-sequencing on tumor samples from 8 DGGH and 8 SGGH patients, complemented by a suite of assays including ELISA, immuno-histochemistry, -blotting and -fluorescence, qPCR, MeRIP, RIP, and RNA stability experiments, aiming to delineate the influence of m^{6}A on tumor behavior. We further assessed the therapeutic potential of targeted drugs using cell cultures, organoid models, and animal studies.

Results We discovered a significant reduction of m^{6}A levels in SGGH compared to DGGH, with an elevated expression of fat mass and obesity-associated protein (FTO), an m^{6}A demethylase, in SGGH subtype. Series of in vivo and in vitro experiments demonstrated that FTO inhibition in tumor cells robustly diminishes hypoxia resistance, attenuates growth hormone secretion, and augments responsiveness to octreotide. Mechanically, FTO-mediated

[†]Yunzhi Zou, Xiaoqiong Bao, Depei Li and Zhen Ye contributed equally to this work.

*Correspondence:
Aiqun Liu
179624095@qq.com
Jialiang Zhang
zhangjial@sysucc.org.cn
Zhixiang Zuo
zuozhx@sysucc.org.cn
Xiaobing Jiang
jiangxiaob1@sysucc.org.cn

Full list of author information is available at the end of the article

m^{6}A demethylation destabilizes desmoplakin (DSP) mRNA, mediated by the m^{6}A reader FMR1, leading to prohibited desmosome integrity and enhanced tumor hypoxia tolerance. Targeting the FTO-DSP-SSTR2 axis curtailed growth hormone secretion, therefor sensitizing tumors to octreotide therapy.

Conclusion Our study reveals the critical role of FTO in the aggressive growth hormone-secreting pituitary neuroendocrine tumors subtype and suggests FTO may represent a new therapeutic target for refractory/persistent SGGH.

Keywords Growth hormone-secreting pituitary neuroendocrine tumors, Pathological classification, N^6-methyladenosine, Desmosome

Background

Growth hormone-secreting pituitary neuroendocrine tumors comprise approximately 10% of pituitary neuroendocrine tumors (PitNETs), which rank among the most prevalent intracranial tumors in adults [1]. Growth hormone-secreting pituitary neuroendocrine tumors are linked to significant comorbidities and increased mortality risk [2]. Prolonged exposure to excessive GH causes detrimental effects on various systems and organs, including the cardiovascular, respiratory, and musculoskeletal systems [3]. Moreover, patients with growth hormone-secreting pituitary neuroendocrine tumors face a significantly higher risk of colorectal, breast, and thyroid cancers. As a result, their long-term quality of life is generally poorer, with a lifespan reduced by approximately 30% compared to the general population [4, 5]. According to the 2022 WHO classification of PitNETs, growth hormone-secreting pituitary neuroendocrine tumors belong to the PIT1 lineage, further divided into densely granulated (DGGH) and sparsely granulated (SGGH) subtypes [6]. DGGH typically exhibits non-invasive growth patterns and has a favorable prognosis. SGGHs are characterized by invasive growth, are resistant to conventional therapies, have poorer prognosis, and are classified as refractory/persistent growth hormone-secreting pituitary neuroendocrine tumors [3, 6]. Despite recent advances in endoscopic techniques, about 15% of growth hormone-secreting pituitary neuroendocrine tumors that invade the cavernous sinus and bone do not achieve a biochemical cure, even with optimal postoperative radiation therapy and update medication [2, 3]. Thus, it is important to explore novel drugs for the treatment of refractory/persistent growth hormone-secreting pituitary neuroendocrine tumors. The distinct biological patterns of DGGH and SGGH serve as a suitable model for investigating the pathogenesis of aggressive behavior.

Desmosomes, comprising various junction proteins, act as vital intercellular junctions that facilitates cellular communication and maintain junctional integrity [7]. Studies have shown that desmosomes play an important role in the development and progression of various malignancies, including gastric, colorectal, and breast cancers. In contrast, the loss or weakening of desmosome structures promotes tumor invasion and metastasis [7]. Within the desmosome complex, desmoplakin (DSP) is a core protein in cell junctions, interacting with other proteins such as plakoglobin, desmoglein, and plakophilin [7]. In cardiac pathologies, mutations in the *DSP* gene impair intercellular desmosome function, contributing to the development of arrhythmogenic cardiomyopathy [8]. In addition, the loss of DSP disrupts intercellular junctions between tumor cells, promoting tumor cell invasion and metastasis [7]. A previous study found that transcripts of genes associated with desmosomal structure and function were consistently downregulated in SGGH, suggesting a critical role of desmosomes in the formation of invasive phenotypes [9].

N^6-methyladenosine (m^{6}A) modification is the most abundant endogenous RNA modification in eukaryotes. It has been reported to participate in various physiological processes, including embryonic development, immune system maturation, and neural development [10]. Through the action of RNA methyltransferases and demethylases, m^{6}A recruits specific reader proteins to target RNAs, thereby influencing RNA stability, translation, alternative splicing, and other functions [11]. Recent studies have demonstrated that the dysregulation of m^{6}A is associated with tumor initiation, invasion, and the formation of cell adhesion [12, 13]. For instance, the m^{6}A demethylase FTO affects metastasis and invasion of Epstein-Barr virus-associated gastric cancer via an m^{6}A-FOS-IGF2BP1/2-dependent manner, providing biomarkers for metastatic prediction and therapy of gastric cancer [14]. FMR1, a novel m^{6}A reader, is upregulated in colorectal cancer (CRC) and plays a critical role in promoting CRC cell proliferation and metastasis by recognizing the m^{6}A-modification site in EGFR mRNA [15]. Additionally, METTL14 influences neuronal activity and pain sensitivity through the GluN2A subunit of NMDAR in chemotherapy-induced neuropathic pain, highlighting a potential therapeutic target for pain management in cancer treatment [16]. However, minimal studies have shown that METTL3 is upregulated in growth hormone-secreting pituitary neuroendocrine tumors and promotes the proliferation and invasiveness of tumor cells [17]. The role of m^{6}A in the pathogenesis of growth

hormone-secreting pituitary neuroendocrine tumors remains to be elucidated.

Our previous studies uncovered the potential function of epigenetic regulation in the progression of invasive PitNETs [18, 19]. Based on these findings, we further analyzed the m^{6}A modifications in DGGH and SGGH samples to explore the role of m^{6}A modification in regulating the aggressive behavior of growth hormone-secreting pituitary neuroendocrine tumors. We identified a distinct m^{6}A profile between DGGH and SGGH, primarily regulated by FTO. By diminishing the mRNA stability of *DSP*, a crucial component of the desmosome, FTO disrupts the desmosome structure and promotes hypoxic tolerance, octreotide resistance and growth hormone secretion of growth hormone-secreting pituitary neuroendocrine tumors. In summary, we propose a novel pathway for distinguishing growth hormone-secreting pituitary neuroendocrine tumors subtypes and reveal the potential pathogenesis of their aggressive growth pattern. The components in this pathway represent potential therapeutic targets for refractory/persistent growth hormone-secreting pituitary neuroendocrine tumors.

Methods

Samples preparation

Our study was conducted in accordance with the guidelines of the Declaration of Helsinki. All data were anonymously analyzed. A total of 39 cases of DGGH and 30 cases of SGGH were included in this study. Among them, 8 DGGH and 8 SGGH samples were recruited for high-throughput m^{6}A-sequencing. The information for the 69 cohorts and high-throughput m^{6}A-sequencing samples is in Table S1-S2. The patients were enrolled at Sun Yat-sen University Cancer Center (Guangzhou, China) from 2018 to 2021. Each patient signed an informed consent form. Ethical approval was obtained from the Medical Ethics Committee of Sun Yat-sen University Cancer Center (G2023-271). Before undergoing endoscopic sinus surgery, no treatments were given. The diagnosis of growth hormone-secreting pituitary neuroendocrine tumors was confirmed through histopathological and biochemical testing. Subtypes were classified based on fibrous bodies according to the latest consensus guidelines (Fig. S1a-b) [6]. DGGH has perinuclear cytokeratin expression, and SGGH shows a predominant (>70%) fibrous body pattern.

High-throughput m^{6}A-sequencing

Total RNA was isolated using TRIzol reagent (Invitrogen, USA) following the manufacturer's procedure. The RNA amount and purity of each sample were quantified using NanoDrop ND-1000 (NanoDrop, USA). The RNA integrity was assessed by Bioanalyzer 2100 (Agilent, CA, USA) with RIN number>7.0, and confirmed by electrophoresis with denaturing agarose gel. Poly (A) RNA was purified from 30 μg total RNA using Dynabeads Oligo (dT)25-61005 (Thermo Fisher, USA) using two rounds of purification. The poly(A) RNA was fragmented into small pieces using the Magnesium RNA Fragmentation Module (NEB, cat.e6150, USA) under 86℃ for 7 min. Then the cleaved RNA fragments were incubated for 2 h at 4℃ with m^{6}A-specific antibody (Synaptic Systems, cat.202003, Germany) in IP buffer (50 mM Tris-HCl, 750 mM NaCl and 0.5% Igepal CA-630). The IP RNA was reverse-transcribed by SuperScript™ II Reverse Transcriptase (Invitrogen, cat.1896649, USA) to generate the cDNA which was then used to synthesize U-labeled second-stranded DNAs with E. coli DNA polymerase I (NEB, cat.m0209, USA), RNase H (NEB, cat.m0297, USA) and dUTP Solution (Thermo Fisher, cat.R0133, USA). An A-base was then added to the blunt ends of each strand, preparing them for ligation to the indexed adapters. Each adapter contains a T-base overhang for ligating the adapter to the A-tailed fragmented DNA. Single- or dual-index adapters were ligated to the fragments, and size selection was performed with AMPureXP beads. After the heat-labile UDG enzyme (NEB, cat.m0280, USA) treatment of the U-labeled second-stranded DNAs, the ligated products were amplified by PCR with the following conditions: initial denaturation at 95℃ for 3 min; 8 cycles of denaturation at 98℃ for 15 s, annealing at 60℃ for 15 s, and extension at 72℃ for 30 s; and then final extension at 72℃ for 5 min. The average insert size for the final cDNA library was 300±50 bp. At last, we performed the 2×150 bp paired-end sequencing (PE150) on an Illumina Novaseq™ 6000 (LC-Bio Technology Co., Ltd., Hangzhou, China).

Processing of MeRIP-seq and RNA-seq data

FastQC (https://www.bioinformatics.babraham.ac.uk/projects/fastqc/) and fastp [20] were employed to perform quality control and preprocessing of raw sequencing reads.

For MeRIP-seq data, analysis was performed using MeRIPseqPipe [21]. Clean reads were aligned to the hg38 genome using STAR [22]. MACS2 [23] (-p 1e-6 --keep-dup 5) and MetPeak [24] were used to identify m^{6}A enriched peaks. The intersect peaks were retained for subsequent analysis. The read coverage of IP and Input data for each peak was calculated using Multicov [25] and normalized by the RPKM method. The radio of IP RPKM (with adding 1) and INPUT RPKM (with adding 1) was used to represent the methylation level of each m^{6}A peak. FeatureCounts [26] was used to generate gene counts. For differential methylation analysis, the Wilcox test was used to examine the significant differences, while DESeq2 [27] was used to identify differentially expressed genes. The m^{6}A peak annotation was performed with the

human annotation file (GENCODE, version 39) downloaded from the GENCODE database (https://www.gencodegenes.org/) using our custom Perl scripts HOMER [28] was performed to find the m^6A motifs.

For scRNA-seq data, raw sequencing data were processed with CellRanger (10X Genomics, v3.1.0) using default settings and aligned to the human genome (GRCh38). Feature-barcode matrices were then treated with CellBender (default parameters) to eliminate ambient RNA. The resulting clean matrices were analyzed using Seurat (v4.1.0). The specific methods involved in scRNA-seq analysis include the preparation of tumor samples and other analyses such as identifying differentially expressed genes (DEGs) and cell classification, and pathway enrichment analysis as previously described [29].

For RNA-seq data, clean reads were aligned to the Rn6 genome using STAR [22]. FeatureCounts was performed to quantify the expression of genes. DESeq2 was used to identify differentially expressed genes and clusterProfiler was used to do the pathway enrichment. Pathway activity was predicted through GSVA and ssGSEA analysis.

Cell lines and cell culture

The human growth hormone-secreting pituitary neuroendocrine tumor cells were isolated from primary growth hormone-secreting pituitary neuroendocrine tumors as described previously and cultured in DMEM/F12 medium (Gibco, NY, USA) supplemented with 20% FBS [19]. The rat growth hormone-secreting pituitary neuroendocrine tumors cell line GH3, which are more likely to be an in vitro model of sparsely granulated subtypes [9], was obtained from the National Infrastructure of Cell Line Resource. GH3 cells were cultured in Dulbecco's modified Eagle's medium (DMEM)/high glucose supplemented with 10% fetal bovine serum (FBS) (Gibco, USA), 100 U/mL penicillin, and 100 μg/mL streptomycin. All cultured cells were maintained at 37 °C in a humidified atmosphere of 5% CO_2. All cell lines used in this study were tested and confirmed to be free of mycoplasma contamination.

RNA isolation and quantitative reverse transcription polymerase chain reaction (qRT–PCR)

Total RNA was extracted from tissues and cells using TRIzol (Invitrogen, USA) following the provided protocol from the manufacturer. Subsequently, the total RNA was reverse-transcribed into complementary DNA (cDNA) utilizing a Reverse Transcription System Kit (Takara BIO INC, Kusatsu, Shiga, Japan). For quantitative real-time PCR, the cDNA served as the template and was amplified using specific primers and a SYBR Premix Ex Taq RNAse H kit (Takara Bio, Tokyo, Japan) in conjunction with the Roche LightCycler 480II detection system. The amplification protocol consisted of an initial 5-minute incubation at 95 °C, followed by 40 cycles of 10 s at 95 °C and 30 s at 60 °C. Each experiment was replicated at least three times. The resulting data were analyzed using the delta-delta CT method (formula: $2^{-(\text{Ct target}-\text{Ct reference})}$) to calculate relative expression levels, which were then compared to control samples. The primers used are listed in Table S3.

m^6A immunoprecipitation (MeRIP)

The total RNA was extracted using the method mentioned above. Specifically, 100 μg of total RNA was subjected to the MERIP experiment using the riboMeRIPTM m^6A Transcriptome Profiling Kit (Ribobio, C11051-1), following the manufacturer's protocol. After immunoprecipitation, the enrichment of RNA was examined using qPCR analysis.

m^6A ELISA

We used the enzyme-linked EpiQuik m^6A RNA methylation quantification kit (Epigentek, NY, USA) to detect the level of m^6A RNA methylation in RNA according to the manufacturer's instructions. Briefly, the control sample and test sample were incubated at 37℃ for 90 min to complete RNA binding, and the capture antibody solution was added and incubated at room temperature for 1 h. Next, the detection antibody solution was added and incubated at room temperature for 30 min to complete RNA capture. Finally, the developer was added and incubated at room temperature for 10 min. When the color of the positive control well changed to moderate blue, the stop solution was added to each well and the absorbance value at 450 nm was measured using an enzyme-linked immunosorbent assay (ELISA) reader. m^6A %= (Sample OD value - NC OD value)÷RNA input/ (Positive control OD value - Negative control OD value)÷Positive control input.

RNA-Binding protein immunoprecipitation (RIP)

Wash freshly resected whole tissue three times with ice-cold PBS. Tumor cells were collected using the primary tumor cell isolation method described above [19]. Collect cells by centrifugation at 1500 rpm for 5 min at 4 °C and discard the supernatant. Subsequently, RIP experiments were performed using the Magna RIP™ RNA-Binding Protein Immunoprecipitation Kit (Millipore, Catalog No. 17–700). After immunoprecipitation, the enrichment of RNA was examined using qPCR analysis.

Immunohistochemistry

The tissues were fixed in 4% paraformaldehyde (PFA) for 24 h and then processed for paraffin embedding. Sectioning was performed at a thickness of 3 mm. Subsequently, the slides underwent deparaffinization and rehydration.

To retrieve the heat-induced epitopes, the slides were submerged in an antigen-unmasking solution (Solarbio). To eliminate endogenous peroxidase and nonspecific binding sites, a sequential treatment with 0.3% H_2O_2 and 5% normal goat serum was carried out. Then antibodies were applied overnight at 4 °C (Table S4). Afterward, the slides were incubated with Dako REAL EnVision HRP rabbit/mouse (belonging to K5007, DAKO, Glostrup, Denmark) for 20 min at room temperature. To visualize the staining signals under light microscopy, Dako REAL DAB+CHROMOGEN and Dako REAL substrate buffer (belonging to K5007, DAKO, Glostrup, Denmark) were applied. Finally, the slides were counterstained using a hematoxylin solution. The stained slides were scanned using KFBIO Digital Pathology Slide Scanners (KFBIO, Ningbo, China) and analyzed with the Halo platform.

Western blot assays

Protein extracts were obtained from tumor tissues or cells by using RIPA buffer (Epizyme Biotech, PC101). The protein concentration was determined using a BCA protein assay kit from Thermo Fisher Scientific. After electrophoresis, proteins were transferred onto PVDF membranes and incubated overnight at 4 °C with the corresponding antibody (Table S4). Subsequently, the membranes were exposed to HRP-conjugated secondary antibodies (1:10000, Abcam, Cambridge, MA, USA) for 1 h at room temperature. The signals were detected using an ECL detection system from Bio-Rad Laboratories (Richmond, CA, USA).

RNA interference

The cells were seeded in six-well plates to reach a density of approximately 50–60% before transfection. 125 μL Opti MEM serum reducing medium (Gibco, Grand Island, NY, USA) containing the required amount of siRNA and Lipofectamine 3000 (Thermo Fisher Scientific, Waltham, MA, USA) was added respectively to two centrifuge tubes and incubated at room temperature for 10 min to form a transfection complex. Evenly add the transfection complex to the six-well plates and perform functional experiments after 48 h of transfection. The sequences of siRNA are listed in Table S5.

Stable cell line generation

Culture 293T cells to achieve a cell density of 70% for transfection. Mix the lentiviral vector with packaging plasmids PSPAX2 and pMD2. G in a 4:3:1 ratio and add them into the medium of 293T cells. 48 h and 72 h later, the virus was collected. Target cells at a density of 70% were incubated with virus and 0.001% polybrene and 48 h later 2 ug/ml puromycin was used to select transduced cells. The sequences of shRNA are listed in Table S5.

RNA stability assays

Cells with or without knockdown of *FTO* or *FMR1* were subjected to treatment with actinomycin D at a final concentration of 2 μM for various time points. Subsequently, total RNA was extracted using the TRIzol reagent. The expression levels were assessed using RT-qPCR, and the mRNA half-life was calculated.

Flow cytometry

Cellular apoptosis of GH3 and primary cells before and after knockdown of FTO and DSP under normal cell culture oxygen concentration or hypoxic environment (1% O_2) were analyzed by flow cytometry using an Annexin V Alexa Fluor 647/7AAD assay kit (Cat: FXP147, 4 A Biotech) according to the manufacturer's instructions and analyzed with a Beckman flow cytometer (Beckman Coulter, Miami, FL, USA).

Cell viability assay

Cell viability was assessed by using CCK-8 assays (DOJINDO, CK04). Following transfection, GH3, and primary cells were seeded in 96-well plates at a density of 5×10^3 cells/well. On days 0, 1, 2, 3, and 4, 10 μl of CCK-8 solution was added to each well and incubated for 2 h. The absorbance at 450 nm was then measured using a Multiskan plate reader. To investigate the influence of FB23-2 (MCE, HY-127103) and OCT (MCE, HY-P0036) on growth hormone-secreting pituitary neuroendocrine tumor cell viability, GH3 and primary tumor cells were seeded into 96-well plates at a density of 5×10^3 cells/well and 2×10^4 cells/well, respectively. After 24 h, the cell medium was changed to a medium containing FB23-2 (4 μM) or OCT (100 nM) or their combination. Three days later, the absorbance was measured as mentioned above.

Colony formation assays

To conduct the cell colony formation assays, 5×10^2 GH3 with FTO knockdown were seeded into 6-well plates and incubated at 37 °C with 5% CO_2. Approximately 10 days later, the cells were washed twice with PBS and fixed with methanol for 30 min. Subsequently, the cells were stained with 0.2% crystal violet for 30 min, and gently washed. The number of colonies was counted.

Growth hormone detection

Growth hormone concentrations in the culture medium of GH3 cells, as well as in serum, were assessed with ELISA kits from Millipore (EZRMGH), following the protocols provided by the manufacturer. Similarly, growth hormone concentrations in the culture medium of primary tumor cells and organoids were determined using a different set of ELISA kits from Elabscience (E-EL-H0177). The growth hormone levels were then

normalized against the results from cell and organoid viability tests, as well as the weight of the tumors.

Organoid culture and drug response assay

Tumor samples were washed and minced, then dissociated and cultured into organoids using specific kits and media. After centrifugation, cells were mixed with Matrigel, deposited into plates, and incubated. Successful organoid formation was monitored by morphology and viability. Organoids larger than 100 μm were used for drug screening and passage. Recurring organoids were dissociated, collected, and cultured again. Drug screening used a modified medium without Y-27,632 on first-generation PDOs. Organoids were dissociated, mixed with Matrigel/modified medium, and seeded into Laminin-coated 384-well plates. After 48 h, a medium containing FB23-2 (4 μM) or OCT (100 nM) or their combination was added. After 4 days, viability was assessed with CellTiter-Glo 2.0, normalizing relative luminescence units to DMSO controls (100% viability) as previously reported [30]. All organoids used in this study were tested and confirmed to be free of mycoplasma contamination.

Animal experiments

BALB/c nude mice aged 4–5 weeks were obtained from Beijing Vital River Laboratory Animal Technology. Each group of mice (five mice per group) received subcutaneous injections of 3×10^6 GH3 cells suspended in 100 μl of PBS into the left axilla area. Tumor volume was measured and calculated using the formula: volume=length × width$^2\times0.5$. Mice were monitored regularly for signs of the defined end-point criteria. To observe the effect of OCT on tumors, once the tumors are visible to the naked eye, daily intraperitoneal injections of the drug (OCT, 50 μg/kg) were initiated. If the weight loss of any mouse exceeded 20% of the initial weight, breathing difficulties, or tumors approaching 15 mm in diameter, it was euthanized immediately and no tumors exceeded this size limit. The Institutional Animal Care and Use Committee of Sun Yat-sen University Cancer Center approved all animal experiments (Ethics Approval no: L102022020004Y), and the handling of the animals adhered to institutional guidelines.

Electron microscopy

Cells were collected by centrifugation and mixed with TEM fixative at 4℃ for 2–4 h, and stored at 4℃. Next, the agarose pre-embedding step was performed. After centrifugation and removal of the supernatant, the samples are washed with 0.1 M phosphate buffer (pH 7.4) and embedded in a 1% agarose solution. Subsequently, post-fixation was done with a 1% osmium tetroxide in 0.1 M phosphate buffer (pH 7.4), fixed at room temperature in the dark for 2 h. Dehydration involved sequential dehydration with different concentrations of alcohol, followed by two dehydration steps with 100% acetone. Permeation and embedding were performed with acetone and EMBed 812, followed by overnight baking at 37℃, and polymerization in an oven at 60℃ for 48 h. The resin blocks were cut into ultrathin sections of 60–80 nm using an ultramicrotome. Finally, staining was conducted with uranyl acetate and lead citrate, and the samples were observed and imaged under a transmission electron microscope for analysis.

Statistical analysis

Statistical analyses were conducted using R 4.1.3 and GraphPad Prism 8.4.2 (San Diego, CA, USA). To ensure biological accuracy, each experiment was replicated independently at least three times. For data following a normal distribution, results were analyzed using Student's t-test. Non-normally distributed data were assessed using the Wilcoxon rank-sum test. Statistical significance was established at a p-value of less than 0.05. All tests were two-sided.

Results

FTO is the key factor leading to distinct m^{6}A levels between different growth hormone-secreting pituitary neuroendocrine tumor subtypes

Firstly, we conducted MeRIP-seq and RNA-seq on 16 tumor samples from 16 individuals with growth hormone-secreting pituitary neuroendocrine tumors, including 8 SGGHs and 8 DGGH (Fig. 1a). Upon merging the m^{6}A peaks from different subtypes, we obtained 48,528 m^{6}A peaks for further analysis. The data showed that most genes exhibited a single m^{6}A peak, and the identified m^{6}A peaks were predominantly enriched in the classical GGACH motif (Fig. 1b). In line with previous studies, these m^{6}A peaks were primarily localized within the coding sequence (CDS) regions and the regions near stop codons, with mRNA being the most enriched molecular form (Fig. 1c-e) [31]. Differential methylation analysis revealed that there were 8,660 (60.94%) hypo-methylated m^{6}A peaks and 5,551 (39.06%) hyper-methylated m^{6}A peaks in SGGHs compared to DGGH, indicating that SGGHs experienced a global decrease in m^{6}A modification (Fig. 1f). Subsequent quantification of global m^{6}A levels using ELISA assays confirmed these lower m^{6}A modification levels in SGGH compared to DGGH (Fig. 1g). Through integrated analysis of m^{6}A modification levels and gene expression profiles, we observed a positive correlation between m^{6}A modification levels and gene expression in growth hormone-secreting pituitary neuroendocrine tumors (Fig. 1h). Our findings revealed distinct m^{6}A modification landscapes between SGGH and DGGH, characterized by a

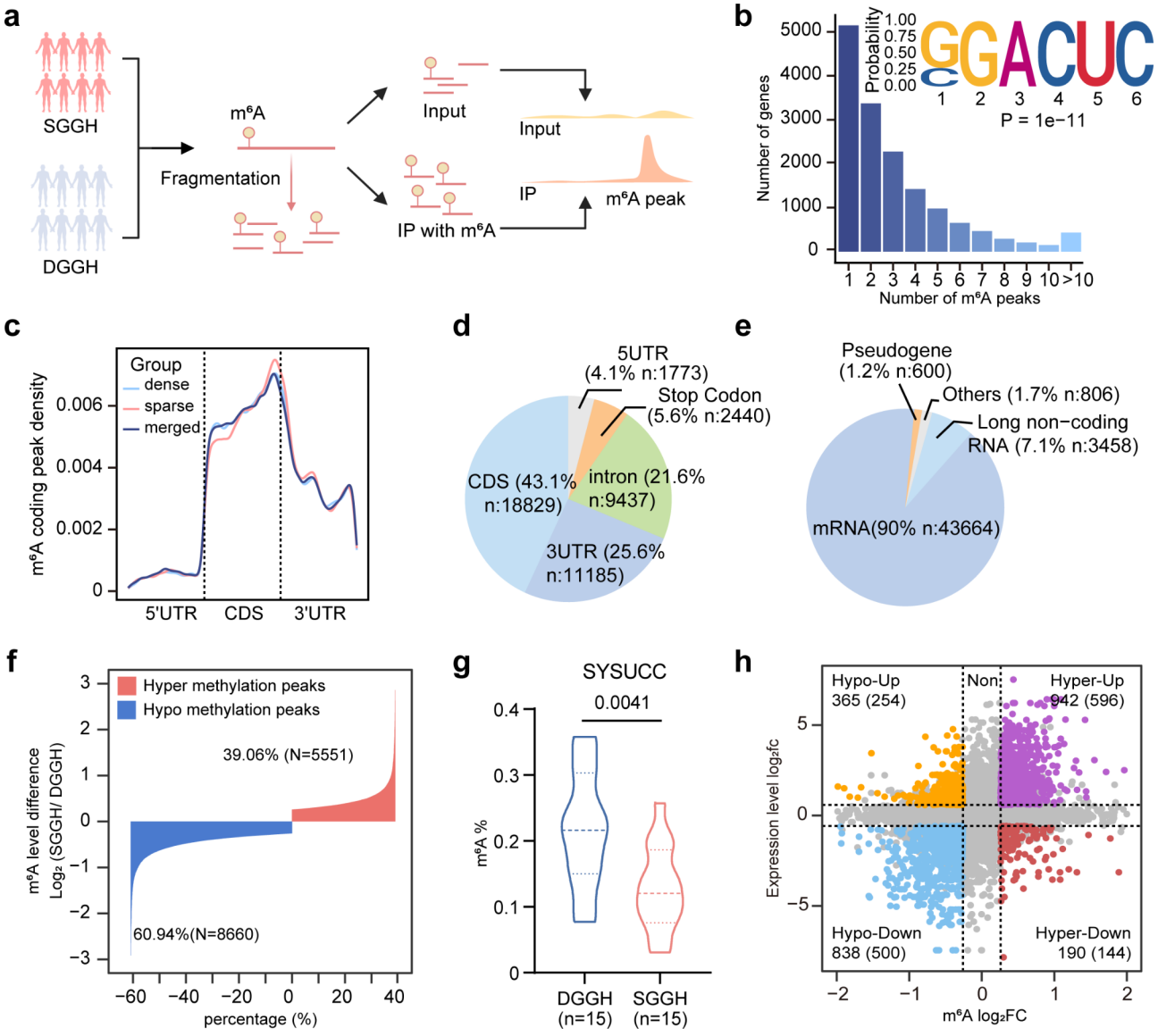

Fig. 1 The m^{6}A modification landscape between subtypes of growth hormone-secreting pituitary neuroendocrine tumors. (**a**) Schematic representation of m^{6}A -seq workflow comparing DGGH and SGGH samples. Eight samples in each group. (**b**) Bar plot of the distribution of m^{6}A peaks across the genome with the predominant m^{6}A motif. (**c**) The distribution of m^{6}A sites across mRNA regions. (**d**) the genomic distribution of m^{6}A modifications by region. (**e**) the genomic distribution of m^{6}A modifications by RNA subtypes. (**f**) The distribution of the different methylation levels of dysregulated m^{6}A peaks within subtypes. (**g**) The difference of global m^{6}A methylation levels in DGGH and SGGH through ELISA. Experiment was replicated independently at least three times. (**h**) Scatter plot of m^{6}A modification peak distribution with subtype-specific gene expression changes in 16 samples

pronounced downregulation of m^{6}A levels in SGGH. This alteration in m^{6}A modification may influence gene expression regulation, contributing to the pathogenesis and phenotypic characteristics of growth hormone-secreting pituitary neuroendocrine tumor subtypes.

Next, we investigated which methylase or demethylase might account for the differential m^{6}A levels among the two subtypes. Based on the sequencing data, both *FTO* and *RBM15* were significantly upregulated in the SGGH (Fig. 2a). However, only FTO was confirmed to be consistently upregulated in another cohort of growth hormone-secreting pituitary neuroendocrine tumor patients (DGGH=39, SGGH=30) treated in our center, a public array dataset (DGGH=10, SGGH=10) and a scRNA-seq dataset (DGGH=2, SGGH=2) (Fig. 2b-g). Additionally, we define Knosp 1–2 as non-invasive according to the literature, and define Knosp 3–4 as invasive [32]. *FTO* was significantly overexpressed in invasive growth hormone-secreting pituitary neuroendocrine tumors compared to non-invasive ones (Fig. 2h). We then performed *FTO* perturbation in cell lines and primary tumor cells (Fig. 2i-l). Overexpression of *FTO* led

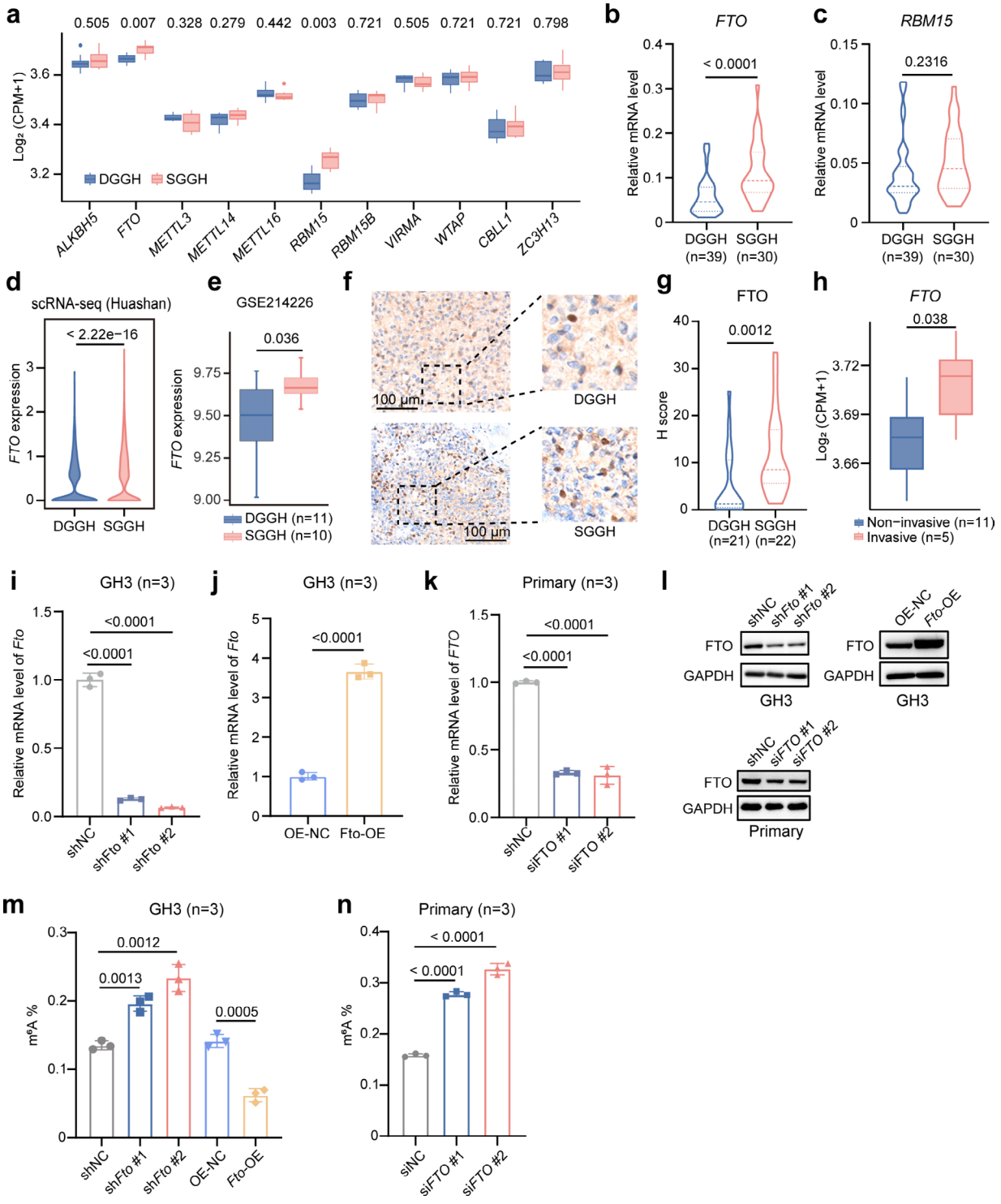

Fig. 2 FTO is the key factor leading to distinct m^{6}A levels among different growth hormone-secreting pituitary neuroendocrine tumor subtypes. **a**. Boxplot of m^{6}A regulatory genes expression between DGGH and SGGH. b-c. Boxplot of quantitative PCR analysis of *FTO* (**b**) and *RBM15* (**c**) level in a cohort of 69 DGGH and SGGH samples. **d**. Violin plot of *FTO* expression in DGGH and SGGH cells in Huashan scRNA-seq cohorts. e. Boxplot showing *FTO* expression levels in DGGH and SGGH based on dataset GSE214226. **f**-**g**. Immunohistochemical staining for FTO in DGGH and SGGH tissue samples. **h**. Boxplot of *FTO* expression between non-invasive and invasive GH adenomas. **i**-**k**. Verification of FTO knockdown and overexpression in GH3 cells and primary tumor cells in mRNA level through qPCR assays. **l**. Western blot assays demonstrating the efficacy of FTO knockdown and overexpression in GH3 cells and primary tumor cells. m-n. Bar plots representing global m^{6}A modification levels following *FTO* manipulation in GH3 cells (**m**) and primary tumor cells (**n**). Each experiment was replicated independently at least three times

to a decrease in overall m^6A levels, while knockdown of *FTO* resulted in an upregulation of m^6A levels (Fig. 1m-n). These findings demonstrate that FTO is the primary demethylase regulating m^6A modifications in different growth hormone-secreting pituitary neuroendocrine tumor subtypes.

Desmosome organization is a key signaling pathway for the aggressive phenotype of SGGH, which is regulated by FTO

Gene expression profiling indicated that multiple pathways related to cell-cell junctions were down-regulated in SGGH (Fig. 3a), specifically desmosome and cell-cell junction organization. Notably, desmosome organization is a subclass of cell-cell junction organization (Fig. S2a). Additionally, scRNA-seq data also demonstrated the significant downregulation of desmosome organization in SGGH (Fig. 3b). DGGH and SGGH were distinctly clustered and separated through PCA analysis, which was based on genes associated with desmosome organization (Fig. 3c, Fig. S2b). ROC analysis revealed that most genes related to desmosome organization possess strong diagnostic capabilities for differentiating DGGH from SGGH (Fig. 3d, Fig. S2c). Genes involved in desmosome organization, including *DSP*, *DSG2*, *PKP2*, and *PKP3*, crucial for cell junctions, were significantly downregulated in SGGH when compared with DGGH (Fig. 3e-f). We tested whether FTO influences the regulation of desmosome organization. Through RNA sequencing and single-sample gene set enrichment analysis (ssGSEA), we found that desmosome organization pathway activity was reduced after *FTO* overexpression and increased following *FTO* knockdown (Fig. 3g). Consistently, desmosome-related genes, including *DSP*, *DSG2*, *PKP2*, and *PKP3*, were downregulated by *FTO* overexpression and upregulated by *FTO* knockdown (Fig. 3h-j). The significant upregulation of functions related to extracellular matrix and angiogenesis is also a characteristic of SGGH. However, overexpression of FTO has no significant effect on the pathway activity of extracellular matrix and angiogenesis. In contrast, FTO knockdown moderately upregulates the pathway activity of extracellular matrix and angiogenesis, which is in conflict with the observed upregulation of extracellular matrix and angiogenesis functions in SGGH (Fig. 3g, S2d-g). To further investigate the functional changes in desmosome organization, we defined desmoglein (DSG) as the marker of desmosome. The DSG protein family is an essential component of desmosome organization, which works as cell surface transmembrane proteins and consists of four members: DSG1, DSG2, DSG3, and DSG4. They are connected to the DSP to form a desmosome or hemidesmosome [33, 34]. Among these members, DSG2 is the only DSG protein that participates in desmosome organization, and it is the crucial component of the desmosome (https://amigo.geneontology.org/amigo/term/GO:0002934). Cell immunofluorescence showed an increase in DSG2 expression on the cell surface after *FTO* knockdown (Fig. 3k). These data further confirm the role of FTO in regulating the dysfunction observed in desmosome organization among growth hormone-secreting pituitary neuroendocrine tumor subtypes.

FTO influences the desmosome organization of growth hormone-secreting pituitary neuroendocrine tumors by regulating the m^6A level of *DSP*

Next, we investigated the specific mechanisms by which FTO affects desmosome organization. Since the global m^6A level in SGGH is lower than that in DGGH, we primarily focused on genes that showed downregulation of m^6A levels. By taking a strict intersection of the differentially expressed genes after *FTO* perturbation, the differentially expressed genes between growth hormone-secreting pituitary neuroendocrine tumor subtypes, and the genes showing downregulation of m^6A levels in SGGH, we found 19 genes that exhibited a negative correlation with *FTO* expression (Fig. 4a). Among these, *DSP* was selected for further analysis since it is a key component of desmosome organization. We found that the level of *DSP* mRNA and protein was significantly decreased in SGGH (Fig. 4b-c). In addition, scRNA-seq data showed significant downregulation of *DSP* in SGGH (Fig. S3a). Consistently, the levels of *FTO* and *DSP* were negatively correlated in two independent datasets (Fig. 4d, Fig. S3b). ROC analysis showed *FTO* and *DSP* possess good diagnostic performance in distinguishing DGGH from SGGH (Fig. 4e, Fig. S2c). In cell lines, *FTO* knockdown and overexpression resulted in upregulation and downregulation of the protein level of DSP, respectively (Fig. 4f-g). To elucidate the regulatory impact of FTO on DSP-mediated desmosome organization, qRT-PCR, western blot and immunofluorescence assays were performed. Our data showed a decrease in both mRNA and protein levels of DSG2 after knocking down *DSP* whereas knocking down *FTO* partially restored the mRNA and protein levels of DSG2 (Fig. 4h-i). Similar results were observed in *PKP2* and *PKP3* (Figs. S3d-f). Immunofluorescence assays demonstrated a reduction of DSG2 expression at the cell surface following the knockdown of *DSP* whereas knocking down *FTO* partially restored the DSG2 expression at the cell surface (Fig. 4j). MeRIP-qPCR further confirmed that the m^6A level on *DSP* in DGGH is significantly higher than that in SGGH (Fig. 4k, S3g). Significantly dysregulated m^6A upon FTO knockdown were further verified by m^6A-sequencing and MeRIP-qPCR (Fig. 4l-n). Taken together, these results provide evidence that FTO is involved in regulating DSP expression through m^6A modification and influencing desmosome function

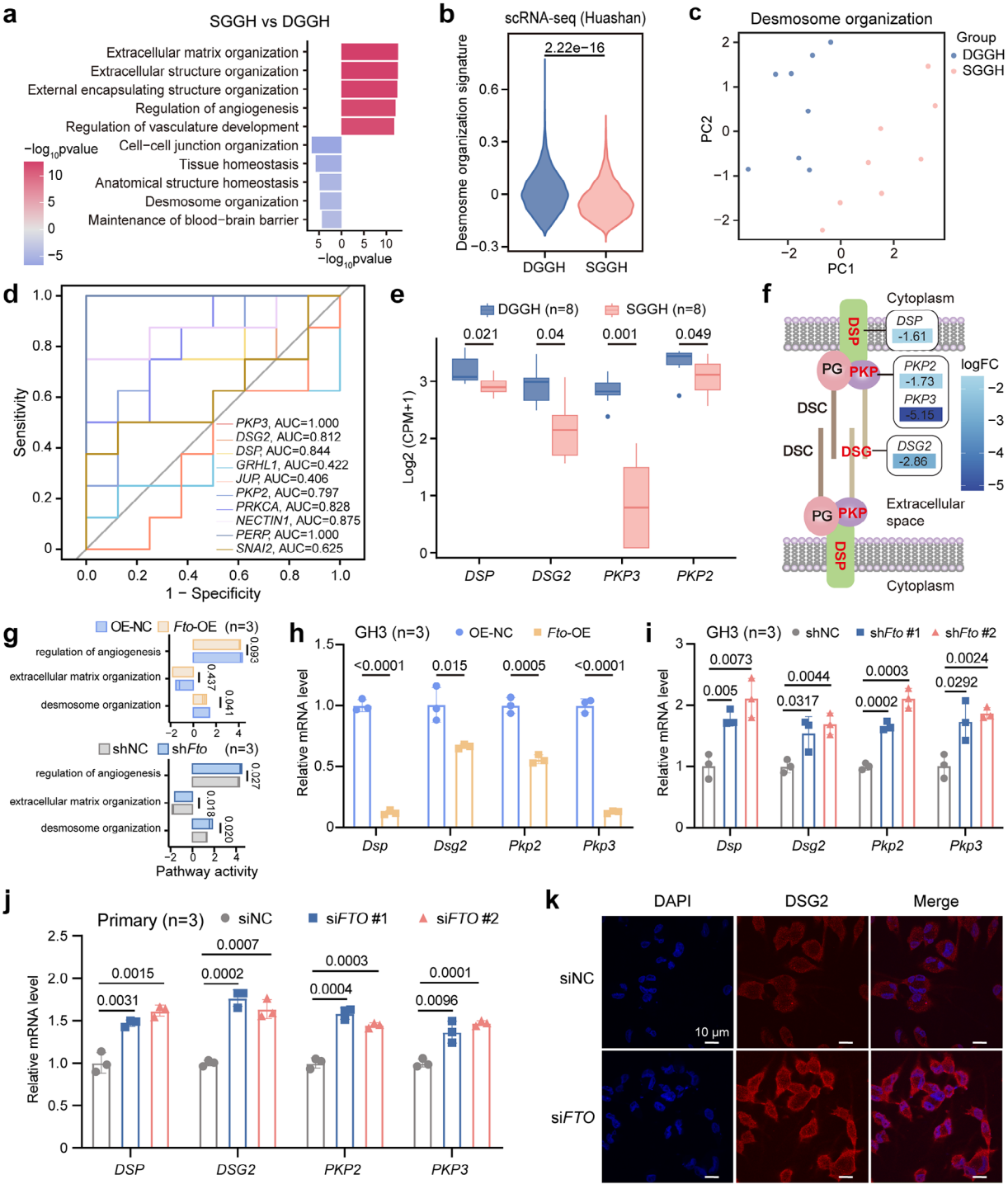

Fig. 3 FTO influences the desmosome organization of growth hormone-secreting pituitary neuroendocrine tumors. **a**. Top five upregulated and downregulated pathways of GO-BP enrichment analysis in SGGH compared with DGGH. **b**. Violin plot showing pathway activity of desmosome organization in DGGH and SGGH cells in Huashan scRNA-seq cohorts. **c**. PCA plot revealing desmosome organization profiling differences between DGGH and SGGH. **d**. ROC curves evaluating the diagnostic performance of desmosome organization related genes in differentiating DGGH from SGGH. **e**. Boxplot showing expression of *DSP*, *DSG2*, *PKP3* and *PKP2* between DGGH and SGGH. **f**. Schematic illustrating downregulated genes of desmosome organization in SGGH. **g**. Pathway activity change of desmosome organization, regulation of angiogenesis and extracellular matrix organization following overexpression (above) and knockdown (below) of *FTO*. **h**. mRNA level changes of *Dsp*, *Dsg2*, *Pkp2* and *Pkp3* following *FTO* overexpression in GH3 cells. **i**-**j**. mRNA level changes of *Dsp*, *Dsg2*, *Pkp2* and *Pkp3* following *FTO* knockdown in GH3 cells (**i**) and primary tumor cells (**j**). k. Immunofluorescence images verified changes in DSG2 protein levels and localization after *FTO* knockdown in primary tumor cells. Each experiment was replicated independently at least three times

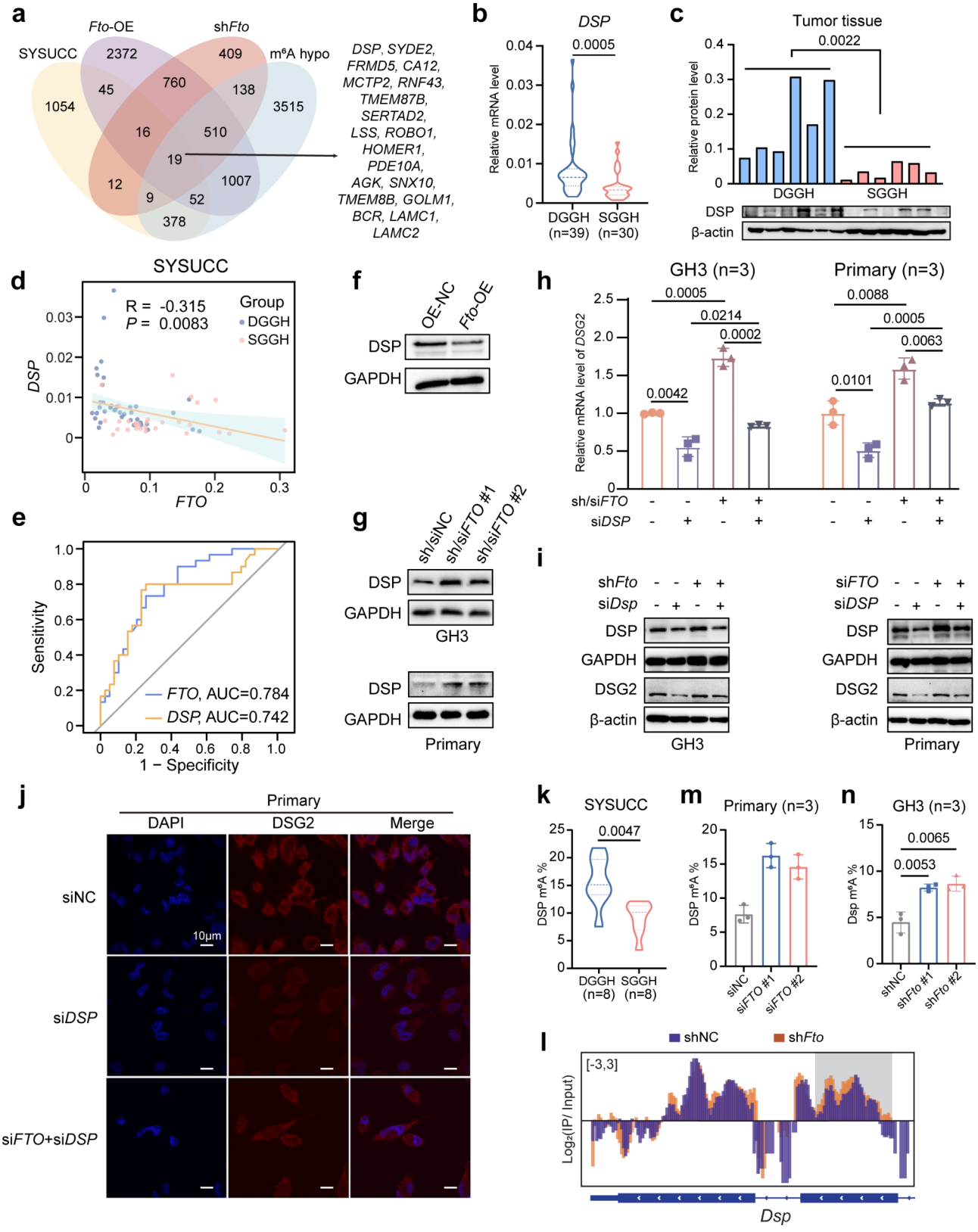

Fig. 4 (See legend on next page.)

(See figure on previous page.)

Fig. 4 FTO influences the desmosome organization of growth hormone-secreting pituitary neuroendocrine tumors through regulating the m^{6}A level of *DSP*. **a**. Venn plot illustrating genes negatively correlated with *FTO* and with downregulated m^{6}A level in SGGH. **b**. Difference of *DSP* mRNA level between DGGH and SGGH sample through qPCR assays in 69 samples. **c**. Western Blotting confirmation of higher DSP protein levels in DGGH tissues. **d**. Regression lines indicating the correlation between *FTO* and *DSP* expression. p and R value were calculated by linear models. **e**. ROC curves evaluating the diagnostic performance of *FTO* and *DSP* in differentiating DGGH from SGGH. **f**. Western blots displaying DSP protein levels following *Fto* overexpression in GH3 cells. **g**. Western blots displaying DSP protein levels following *Fto* knockdown in GH3 cells (above) and primary tumor cells (below). **h**. Changes in mRNA levels of *Dsg2* in GH3 cells and primary tumor cells following *Dsp* and *Fto* knockdown through qPCR assays. **i**. Western blot presenting DSG2 protein expression changes following *Fto* and *Dsp* knockdown in GH3 cells (left) and primary tumor cells (right). **j**. Immunofluorescence images verified changes in DSG2 protein levels and localization following *FTO* and *DSP* knockdown in primary tumor cells (**j**). k. m^{6}A level of *DSP* in DGGH and SGGH through MeRIP-qPCR assays. **l**. Graphical representation of differential m^{6}A modification peaks on the *DSP* after *FTO* knockdown through m^{6}A-seq. m-n. Bar plot demonstrating the impact of *FTO* knockdown on m^{6}A levels of *DSP* in primary tumor cells (**m**) and GH3 cells (**n**) through MeRIP-qPCR assays. Each experiment was replicated independently at least three times

in growth hormone-secreting pituitary neuroendocrine tumors.

FTO regulates the mRNA stability of *DSP* by interacting with m^{6}A reader FMR1

We sought to understand how FTO-mediated m^{6}A modification affects the mRNA level of *DSP*. Since *DSP* mRNA expression positively correlated with its m^{6}A levels (Fig. 4a), we hypothesized that m^{6}A modification might affect the stability of *DSP* mRNA. Upon treatment with actinomycin D, which inhibits de novo RNA synthesis, the stability of *DSP* mRNA increased in *FTO* knockdown and decreased in *FTO* overexpression. (Figs. 5a-c). This suggests that FTO influences the stability of *DSP* mRNA via m^{6}A. Generally, m^{6}A modification regulates mRNA stability through reader proteins, including IGF2BP1, IGF2BP2, and IGF2BP3 [12]. However, DSP mRNA and protein levels were unchanged knocking down these readers (Figs. S4a-d). Subsequently, we utilized SRAMP (https://www.cuilab.cn/sramp/) to identify m6A modification sites based on differential peaks [34] and used the RMVar database (https://rmvar.renlab.org/) to find RNA-binding proteins at those sites [35, 36]. A total of five high-confidence sites and one moderate-confidence site were found. Among them, site 485 is associated with three RNA-binding proteins, FMR1, HNRNPC, and SND1. Site 1038 is associated with two RNA-binding proteins, NUDT21 and ACIN1 (Fig. 5d). In a previous study, FMR1 has been reported to be involved in the regulation of mRNA stability through m^{6}A modifications [37]. Additionally, the expression level of *FMR1* in SGGH tends to be lower than in DGGH (Fig. 5e, Fig. S4e). We subsequently validated the binding of FMR1 to the 485 site using RIP-qPCR. FTO knockdown significantly reduced the binding of FMR1 and m^{6}A on DSP (Fig. 5f). Importantly, our studies show that following knocking down *FMR1*, the mRNA, protein levels, and mRNA stability of *DSP* were decreased (Fig. 5g-j, S3f). The above results suggest that FMR1 acts as a reader protein for m^{6}A modification to regulate *DSP* mRNA stability.

FTO knockdown inhibits hypoxia tolerance and formation of fibrous bodies of growth hormone-secreting pituitary neuroendocrine tumors

To further elucidate the clinical relevance of FTO in managing aggressive growth hormone-secreting pituitary neuroendocrine tumors, we conducted a series of functional experiments using cell lines, primary tumor cells and animal models. FTO does not affect the proliferation or clonal formation of cell lines and primary tumor cells (Fig. 6a-d). Besides, FTO does not affect the tumor volume and weight in subcutaneous tumor formation (Fig. 6e-h). Some research reports that hypoxic conditions may play an important role in pituitary tumorigenesis, and dysfunction in desmosomes may affect the hypoxia tolerance of growth hormone-secreting pituitary neuroendocrine tumor cells [9, 38–41]. We tested the importance of FTO on cell viability under hypoxic conditions (1% oxygen). By performing flow cytometry analysis, we determined that FTO knockdown does not influence cell apoptosis under normoxic conditions, but significantly increases the apoptosis rate under hypoxic conditions. Moreover, *DSP* knockdown elevates cell apoptosis under normoxic conditions but reduces the apoptosis rate under hypoxic conditions (Fig. 6i). Additionally, DGGH and SGGH exhibit pathological differences in fibrous bodies. In the study by Wierman et al., the authors speculated that disruption of desmosome organization may be associated with the formation of these fibrous bodies [9]. Indeed, our electron microscopy studies revealed a sparser distribution of filaments within the fibrous bodies of primary tumor cells following *FTO* knockdown (Fig. 6j).

Targeting FTO reduces the GH-secreting capability of tumor cells and enhances their sensitivity to somatostatin analogs

In clinical settings, patients diagnosed with growth hormone-secreting pituitary neuroendocrine tumors commonly suffer from a variety of systemic complications affecting different organs as a result of excess growth hormone secretion. The primary medications recommended for growth hormone-secreting pituitary neuroendocrine

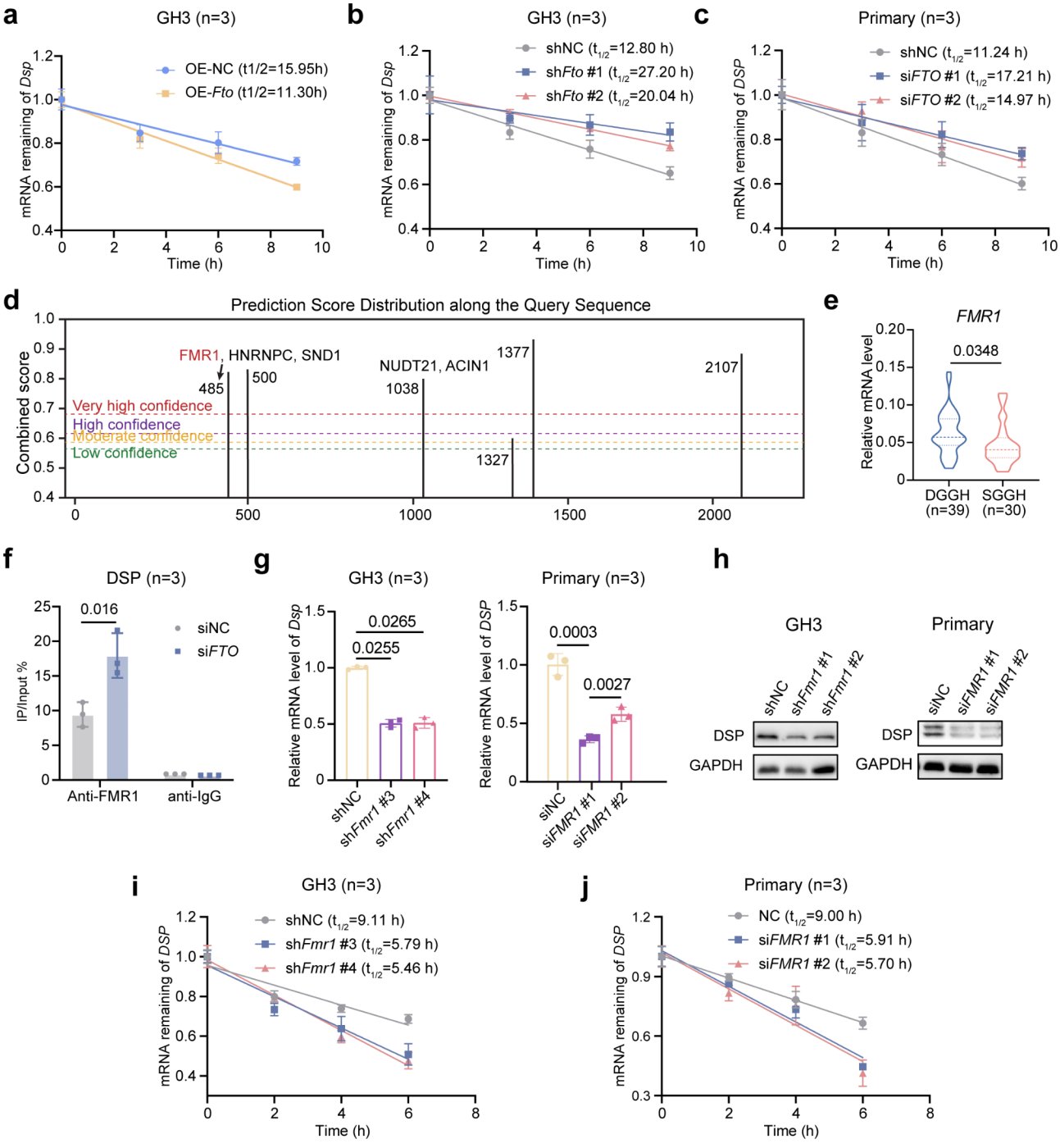

Fig. 5 FTO regulates the mRNA stability of *DSP* by interacting with m^{6}A reader FMR1. a-c. mRNA stability changes of *DSP* after *FTO* perturbation in GH3 cells (**a**-**b**) and primary tumor cells (**c**) after actinomycin D treatment. **d**. Prediction score distributions for m^{6}A modification site with related RNA binding proteins, as determined using the SRAMP prediction tool and RMVar database. **e**. qPCR result show *FMR1* mRNA level in DGGH and SGGH. **f**. Bar plot demonstrating the impact of FTO knockdown on the binding of FMR1 and m^{6}A on DSP through RIP-qPCR. **g**. *DSP* mRNA level change after *FMR1* knockdown in GH3 cells (left) and primary tumor cells (right), quantified by qPCR. **h**. Western blots display DSP protein level alterations after *FMR1* knockdown in GH3 cells (left) and primary tumor cells (right). **i**-**j**. mRNA stability changes of *DSP* after *FMR1* knockdown in GH3 cells (**i**) and primary tumor cells (**j**) under actinomycin D treatment. Each experiment was replicated independently at least three times

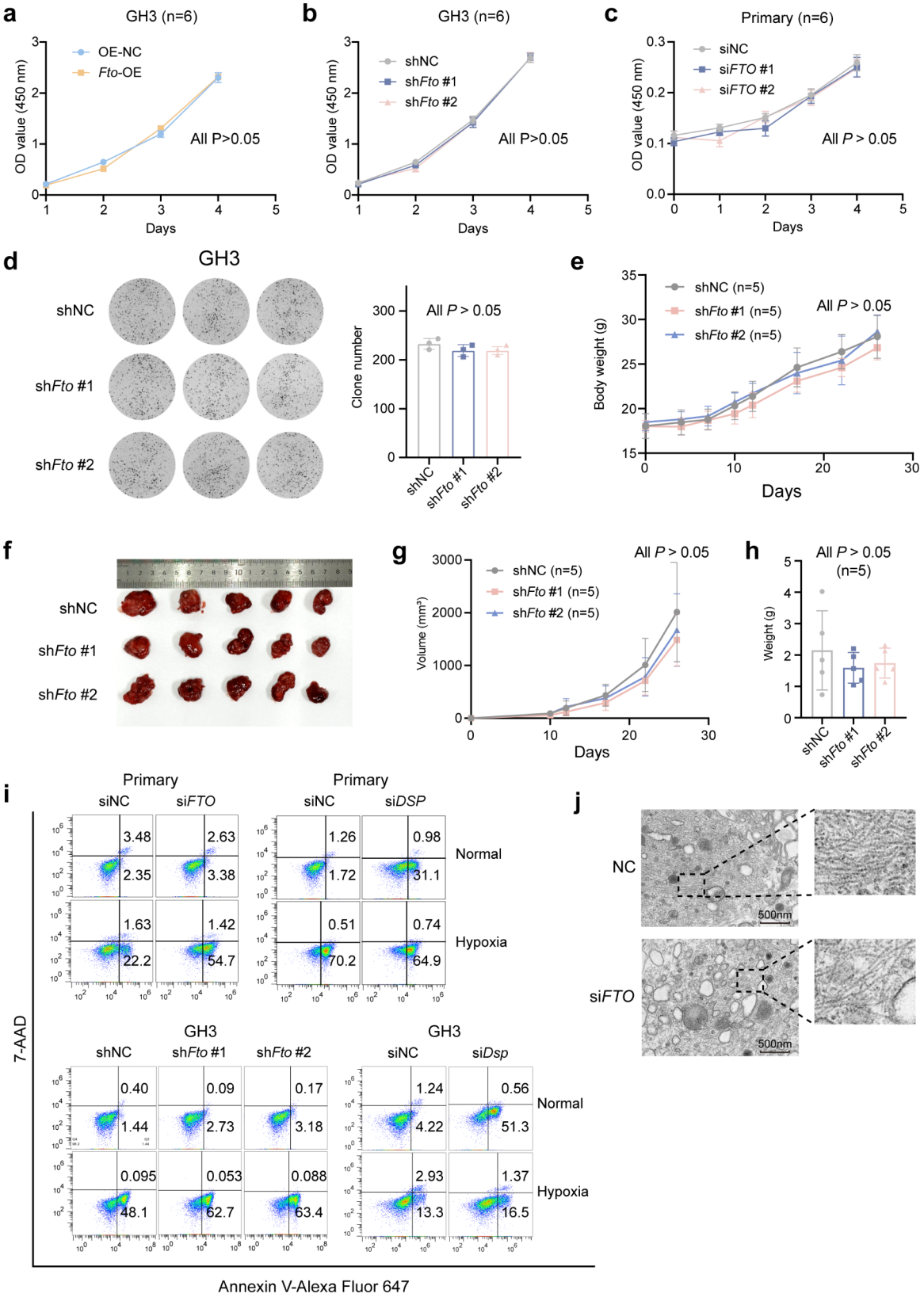

Fig. 6 (See legend on next page.)

(See figure on previous page.)

Fig. 6 *FTO* knockdown influences hypoxia tolerance and formation of fibrous bodies of growth hormone-secreting pituitary neuroendocrine tumors cells. **a**-**c**. Cell viability measured by CCK8 assays in GH3 (**a**-**b**) and primary tumor cells (**c**) cells under *FTO* perturbation. **d**. Colony formation was performed in GH3 cells following *Fto* knockdown. **e**. Line graph detailing changes in mouse body weight over time. **f**. Image of subcutaneous tumors from xenograft model by injecting GH3 cells following *Fto* knockdown. **g**. Detailed changes in mouse. **h**. Bar plot showing the effect of *Fto* knockdown on tumor wight. **i**. Flow cytometry analysis of percentage of apoptosis under normal and hypoxia after *FTO* and *DSP* knockdown in primary tumor cells and GH3 cells. **j**. Electron microscopy images show differences in fiber density within fibrous bodies after *FTO* knockdown in primary tumor cells. Each experiment was replicated independently at least three times

tumor patients are somatostatin analogs, such as octreotide [2]. However, individuals with SGGH often exhibit resistance to these drugs. Therefore, we further assessed the influence of FTO on growth hormone secretion capacity and sensitivity to somatostatin analogs in these patients.

Octreotide treatment for growth hormone-secreting pituitary neuroendocrine tumor primarily works by targeting somatostatin receptor, which downregulates the transcription level of growth hormone, thereby inhibiting its secretion and, to some extent, suppressing the growth of the growth hormone-secreting pituitary neuroendocrine tumors [42–45]. Reduced somatostatin receptor 2 (SSTR2) and elevated somatostatin receptor 5 (SSTR5) expression is a key characteristic of refractory/persistent growth hormone-secreting pituitary neuroendocrine tumors. Therefore, we first examined the impact of FTO on the transcription and protein levels of SSTR2, SSTR5 and growth hormone. RNA sequencing results showed that after FTO knockdown, SSTR2 levels were significantly upregulated, while growth hormone levels were significantly downregulated (Fig. 7a). Additionally, *DSP* has a significant positive correlation with *SSTR2* (Fig. S5a).We subsequently validated these findings using qPCR, western blot, and growth hormone ELISA experiments (Fig. 7b-c, S5b). FTO knockdown can also downregulate the level of SSTR5 (Fig. S5c-d). Electron microscopy demonstrated a decrease in secretory granules after *FTO* knockdown in primary tumor cells derived from a patient with growth hormone-secreting pituitary neuroendocrine tumor (Fig. 7d). Concerning sensitivity to octreotide, knockdown of *FTO* enhances the sensitivity of GH3 and primary tumor cells to octreotide (Fig. 7e). Treatment with FB23-2, a methyltransferase inhibitor of FTO, enhanced the sensitivity of growth hormone-secreting pituitary neuroendocrine tumors organoids and cells to octreotide, and inhibited the secretion of growth hormone (Fig. 7f-h). In subcutaneous tumors, we showed that octreotide inhibited the growth of *FTO*-knockdown cells more effectively and further reduced the secretion of growth hormone (Fig. 7i-l, S5e).

Integrating our results, targeting FTO reduces tolerance in hypoxic microenvironments, inhibites growth hormone secretion function and enhances sensitivity to octreotide in growth hormone-secreting pituitary neuroendocrine tumors. Additionally, it also has some impact on the formation of fibrous bodies (Fig. 8).

Discussion

Growth hormone-secreting pituitary neuroendocrine tumors have significant effects on the body and are associated with various diseases. However, the molecular mechanisms underlying the development and classification differences of these tumors are not yet fully understood. Initial findings suggested that an activating mutation in the G protein subunit A, leading to constant activation of cyclic adenosine monophosphate (cAMP), was associated with DGGH [46]. However, further research revealed that G protein subunit A mutations are present in 40–65% of growth hormone-secreting pituitary neuroendocrine tumors, including 23–38% of SGGH, indicating that these mutations do not align with specific tumor histological subtypes [46–51]. In Ezzat's study, it was found that 43% of SGGH tumors exhibited mutations in the growth hormone receptor (GHR), while no mutations were found in DGGH tumors [52]. However, other research groups did not identify GHR mutations in their study cohorts [49, 53]. In 2017, Wierman's study provided transcriptomic high-throughput data comparing DGGH and SGGH. The study found a consistent downregulation of E-cadherin, SSTR2, and p27 kip in SGGH, indicating enhanced epithelial-mesenchymal transition (EMT) functionality compared to DGGH, which aligned with previous findings [9]. Our dataset al.so confirmed the consistent differences observed in the Wierman study (Figs. S5a-c). Moreover, Wierman's study highlighted that the major difference between DGGH and SGGH lies in desmosome organization. The expression of key desmosome components such as *DSP*, *PKP2*, plakophilin-like protein (*PERP*), and others were significantly downregulated in SGGH, suggesting that alterations in desmosomes may be a crucial factor and may be used for the classification differences between SGGH and DGGH [9]. Desmosomes typically act as tumor-suppressive complexes. The absence of desmosome proteins and desmosome-mediated adhesion is associated with the development and/or progression of cancer [7].

In this study, we aimed to investigate the molecular characteristics of different histological subtypes of growth hormone-secreting pituitary neuroendocrine tumors, specifically focusing on the role of m^6A modification and its impact on desmosome organization. Initially, we conducted m^6A sequencing and observed the downregulation of m^6A levels in the SGGH subtype. We also validated the results using m^6A ELISA, external datasets,

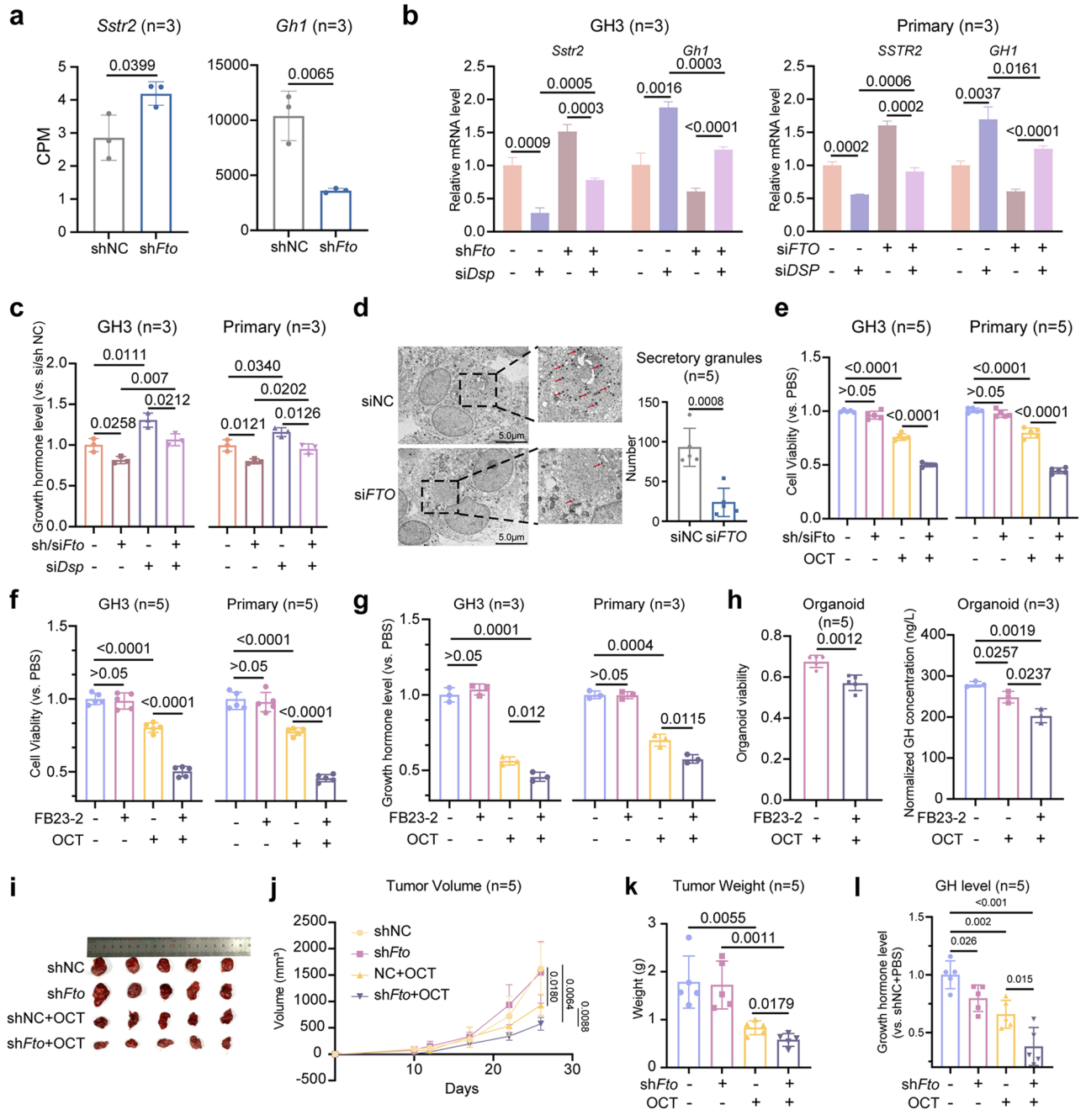

Fig. 7 Targeting FTO reduces GH secreting capability of tumor cells and enhances their sensitivity to somatostatin analogs. **a**. Bar plots showing the *Sstr2* and *Gh1* level change after *Fto* knockdown through RNA-seq analysis. **b**. Bar plots showing the *Sstr2* and *Gh1* level change after *FTO* and *DSP* knockdown in GH3 cells (left) and primary tumor cells (right) through qPCR analysis under the stimulation of octreotide (100nM). **c**. Bar plots showing the growth hormone level changes following *FTO* and *DSP* knockdown in GH3 cells (left) and primary tumor cells (right) under the stimulation of octreotide (100nM). **d**. Electron microscopy showing fewer secretory granules after *FTO* knockdown in primary tumor cells. **e**. Bar plots showing the octreotide sensitivity change after *FTO* knockdown in GH3 cells (left) and primary tumor cells (right). **f**. Bar plots showing the octreotide sensitivity change after combing with FB23-2 treatment in GH3 cells (left) and primary tumor cells (right). **g**. Bar plots showing the growth hormone level changes following octreotide and FB23-2 treatment in GH3 cells (left) and primary tumor cells (right). **h**. Bar plots showing the octreotide sensitivity (left) and growth hormone level (right) change after combining with FB23-2 in organoids. **i**-**j**. In vivo assessment of octreotide sensitivity in GH3 xenografts by injecting with or without *Fto* knockdown GH3 cells according to tumor volume (**j**), tumor weight (**k**) and growth hormone level (**l**). Each experiment was replicated independently at least three times

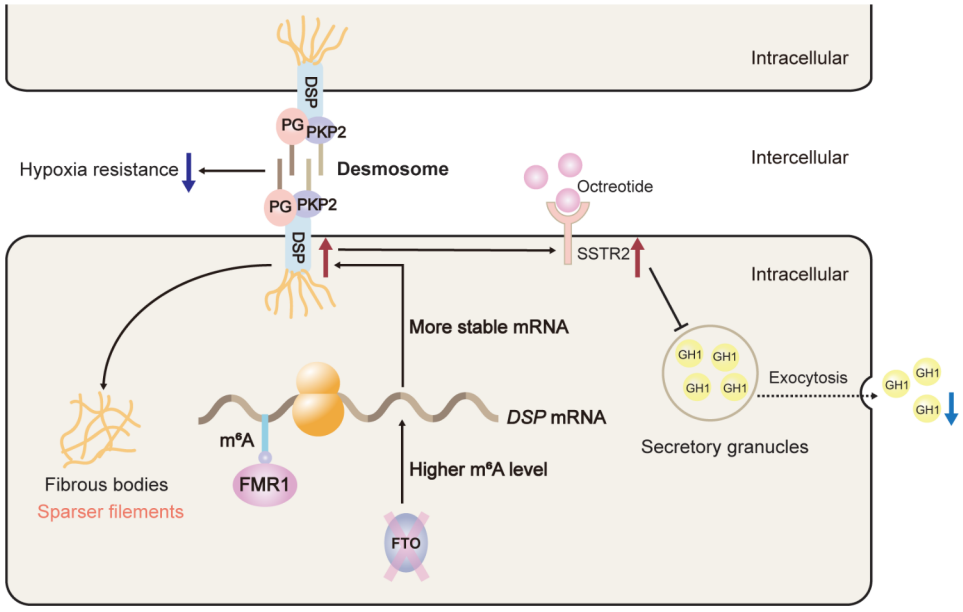

Fig. 8 The schematic model of targeting FTO in the aggressive subtype of growth hormone-secreting pituitary neuroendocrine tumor

and immunohistochemistry. Through these comprehensive analyses, we discovered that FTO was significantly upregulated in SGGH. FTO is known to play a role in regulating m^6A modification levels in mRNA. In our study, we found that FTO regulates the m^6A modification levels of the mRNA encoding the critical desmosomal component DSP. This dysregulation of m^6A modification led to a reduction in desmosome organization in SGGH. Furthermore, we investigated the value of the clinical application of FTO in growth hormone-secreting pituitary neuroendocrine tumors. We found that the downregulation of FTO decreases hypoxia tolerance in pituitary tumor cells. Additionally, we found that *FTO* knockdown upregulated SSTR2 levels, which in turn led to a downregulation of growth hormone synthesis and secretion. Due to the potential relationship between fibrous bodies and desmosomes [9], we also found that *FTO* knockdown also makes the filaments sparser in fibrous bodies. These findings highlight the role of FTO in regulating the malignant phenotype of growth hormone-secreting pituitary neuroendocrine tumors and contribute to a better understanding of the molecular mechanisms underlying the differences between SGGH and DGGH. Our studies suggest that FTO may represent an effective therapeutic target and diagnostic marker for growth hormone-secreting pituitary neuroendocrine tumors. However, further research is needed to fully elucidate the underlying mechanisms and validate the therapeutic potential of targeting FTO.

Notably, desmosome organization is not only the primary difference between the SGGH and DGGH (Fig. 3a) but also plays a significant role in the development of growth hormone-secreting pituitary neuroendocrine tumors. Using GSVA analysis, we observed a downregulation of desmosome organization in growth hormone-secreting pituitary neuroendocrine tumors compared to normal pituitary (Fig. S6a). Additionally, based on AUC analysis, most of the desmosome genes exhibited good discriminatory power in distinguishing growth hormone-secreting pituitary neuroendocrine tumors from normal pituitary samples. Among them, DSP showed remarkable discriminatory power (Fig. S6b). Principal component analysis revealed that desmosome genes can effectively separate growth hormone-secreting pituitary neuroendocrine tumors from normal pituitary samples (Fig. S6c). Besides, through the analysis of gene expression in the brain using the Human Protein Atlas database (https://www.proteinatlas.org/), we discovered genes downregulated in SGGH have a significantly higher expression in the pituitary gland compared with other brain regions, except for the retina (Figs. S6d-g). These results indicate the importance of desmosome organization in pituitary gland, and the alterations in their function are crucial for the onset and development of PitNETs.

There are some areas that deserve attention. Compared to DGGH, the proliferative capacity of SGGH is significantly enhanced. In our study, we found that the disturbance of FTO has no significant effect on the cell proliferation of growth hormone-secreting pituitary neuroendocrine tumors. Since we only performed single-gene interference at the cellular level, our interpretation of the SGGH phenotype is relatively limited. The interactions between cells, extracellular matrix, and angiogenesis functions in the tumor microenvironment may play an important role in the high proliferation of SGGH. Additionally, we found that the number of secretory granules

decreased after FTO knockdown. However, the number of secretory granules in SGGH is less than in DGGH, which is very interesting and important. This contradictory finding might be partly accounted for by the comprehensive regulatory mechanisms of growth hormone secretion. Overall, FTO has the potential to inhibit growth hormone secretion and thereby improve patient prognosis. Many studies have reported that targeting growth hormone secretion can significantly improve treatment outcomes and reduce risks for a range of tumors, including neuroblastomas, glioblastomas, breast cancer, prostate cancer, and non-small-cell lung cancer [54–57]. We will continue to explore these in the future.

Conclusions

Overall, our study demonstrates the significance of FTO-mediated pathogenesis in the aggressive growth hormone-secreting pituitary neuroendocrine tumors and reveals new therapeutic targets. Moreover, the desmosome-associated genes modulated by FTO could function as innovative factors for categorizing growth hormone-secreting pituitary neuroendocrine tumors.

Abbreviations

PitNETs	Pituitary neuroendocrine tumors
DGGH	Densely granulated growth hormone-secreting pituitary neuroendocrine tumors
SGGH	Sparsely granulated growth hormone-secreting pituitary neuroendocrine tumors
m^6A	N^6-methyladenosine
DSP	Desmoplakin
pkp2	Plakophilin 2
PERP	Plakophilin-like protein
CRC	Colorectal cancer
CDS	Coding sequence
ssGSEA	Single-sample gene set enrichment analysis
SSTR2	Somatostatin receptor 2
SSTR5	Somatostatin receptor 5
cAMP	Cyclic adenosine monophosphate
GHR	Growth hormone receptor
EMT	Epithelial-mesenchymal transition

Supplementary Information

The online version contains supplementary material available at https://doi.org/10.1186/s12943-024-02117-5.

Supplementary Material 1

Supplementary Material 2

Acknowledgements

We would like to express our gratitude to other members of Dongxin Lin and Jian Zheng's research group at Sun Yat-sen University Cancer Center for their valuable suggestions on the research design.

Author contributions

Xiaobing Jiang, Zhixiang Zuo, Jialiang Zhang, Zhe Zhu and Aiqun Liu conceived and designed the study. Yunzhi Zou, Depei Li, and Yuanzhong Yang did most of the experiments. Ziming Chen, Lingxing Zeng, Chunling Xue, Hongzhe Zhao, and Ruihong Bai assisted in carrying out the experiments. Xiaoqiong Bao, Yunzhi Zou, Zhen Ye, Rong Xiang, Jixiang Zhao, and Zhenhua Zhang contributed to data processing and analysis. Zhixiang Zuo, Boyuan Yao, and Qilin Zhang supervised the data processing and analysis. Yunzhi Zou, Zhen Ye, Depei Li, Zeming Yan, Zekun Deng, Jintong Cheng, and Guanghao Yue contributed to the sample and information collection. Yuanzhong Yang, Zhe Zhu, and Wanming Hu conducted pathological analysis. Yunzhi Zou, Jialiang Zhang, Xiaoqiong Bao, and Rong Xiang prepared and revised the figures and drafted the manuscript. Xiaobing Jiang and Zhixiang Zuo supervised the research. All authors read and approved the final manuscript.

Funding

This study was supported by the National Natural Science Foundation of China (82372624 to Xiaobing Jiang), Guangdong Basic and Applied Basic Research Foundation (2022A1515012430 and 2024A1515013102 to Xiaobing Jiang, 2021B1515020108 to Zhixiang Zuo), Guangdong Esophageal Cancer Institute Science and Technology Program (M202206 to Zhixiang Zuo) and Young Talents Program of Sun Yat-sen University Cancer Center (YTP-SYSUCC-0062 to Jialiang Zhang).

Data availability

Public RNA-seq datasets for growth hormone-secreting pituitary neuroendocrine tumors are accessible under GEO accessions: GSE214226. Public scRNA-seq datasets for growth hormone-secreting pituitary neuroendocrine tumors are generously provided by Professor Zhao's team at Huashan Hospital (https://pubmed.ncbi.nlm.nih.gov/36754052/). The raw sequence data reported in this paper have been deposited in the Genome Sequence Archive in BIG Data Center, Beijing Institute of Genomics (BIG), Chinese Academy of Sciences [http://bigd.big.ac.cn/] and GEO database under restricted access: HRA007337 (MeRIP-seq for growth hormone-secreting pituitary neuroendocrine tumors samples, https://ngdc.cncb.ac.cn/gsa-human/s/v52im56T for review only), CRA016311 or GSE269321 (MeRIP-seq for GH3 cell line, https://ngdc.cncb.ac.cn/gsa/s/8WVmDLmV or https://www.ncbi.nlm.nih.gov/geo/query/acc.cgi?acc=GSE269321 for review only), CRA016340 or GSE269044 (RNA-seq for GH3 cell line, https://ngdc.cncb.ac.cn/gsa/s/zpBrK8CM or https://www.ncbi.nlm.nih.gov/geo/query/acc.cgi?acc=GSE269044 for review only). The researchers can register and login to the GSA database website [https://ngdc.cncb.ac.cn/gsa-human/] and follow the guidance of "Request Data" to request the data step by step [https://ngdc.cncb.ac.cn/gsa-human/document/GSA-Human_Request_Guide_for_Users_us.pdf] and/or by contacting zuozhx@sysucc.org.cn or jiangxiaob1@sysucc.org.cn. All requests will be reviewed by corresponding authors and the SYSUCC institutional review board. The approximate response time for accession requests is about two weeks. The access authority can be obtained for scientific research and not-for-profit use only. Once access has been granted, the data will be available to download for two months. All data supporting the findings of this work are included in this article and the supplementary materials files.

Declarations

Consent for publication

Not applicable.

Competing interests

The authors declare no competing interests.

Author details

[1]State Key Laboratory of Oncology in South China, Guangdong Provincial Clinical Research Center for Cancer, Sun Yat-sen University Cancer Center, Guangzhou 510060, P. R. China
[2]Department of Neurosurgery, Huashan Hospital, Shanghai Medical College, Fudan University, Shanghai 200040, China
[3]Department of Pathology and Cell Biology, New York-Presbyterian Hospital, Columbia University Irving Medical Center, New York, NY, USA
[4]School of Pharmaceutical Sciences, Sun Yat-sen University, Guangzhou, Guangdong 510006, China
[5]The First Affiliated Hospital of Guangdong Pharmaceutical University, Guangzhou, China

Received: 9 July 2024 / Accepted: 5 September 2024
Published online: 20 September 2024

References

1. Molitch ME. Diagnosis and treatment of Pituitary adenomas: a review. JAMA. 2017;317:516–24.
2. Fleseriu M, Biller BMK, Freda PU, Gadelha MR, Giustina A, Katznelson L, Molitch ME, Samson SL, Strasburger CJ, van der Lely AJ, Melmed S. A Pituitary Society update to acromegaly management guidelines. Pituitary. 2021;24:1–13.
3. Colao A, Grasso LFS, Giustina A, Melmed S, Chanson P, Pereira AM, Pivonello R. Acromegaly. Nat Rev Dis Primers. 2019;5:20.
4. Wu JC, Huang WC, Chang HK, Ko CC, Lirng JF, Chen YC. Natural history of Acromegaly: Incidences, re-operations, cancers, and Mortality Rates in a National Cohort. Neuroendocrinology. 2020;110:977–87.
5. Terzolo M, Reimondo G, Berchialla P, Ferrante E, Malchiodi E, De Marinis L, Pivonello R, Grottoli S, Losa M, Cannavo S, et al. Acromegaly is associated with increased cancer risk: a survey in Italy. Endocr Relat Cancer. 2017;24:495–504.
6. Asa SL, Mete O, Perry A, Osamura RY. Overview of the 2022 WHO classification of Pituitary tumors. Endocr Pathol. 2022;33:6–26.
7. Dusek RL, Attardi LD. Desmosomes: new perpetrators in tumour suppression. Nat Rev Cancer. 2011;11:317–23.
8. Basso C, Bauce B, Corrado D, Thiene G. Pathophysiology of arrhythmogenic cardiomyopathy. Nat Rev Cardiol. 2011;9:223–33.
9. Kiseljak-Vassiliades K, Mills TS, Zhang Y, Xu M, Lillehei KO, Kleinschmidt-DeMasters BK, Wierman ME. Elucidating the role of the desmosome protein p53 apoptosis effector related to PMP-22 in growth hormone tumors. Endocrinology. 2017;158:1450–60.
10. Liu J, Dou X, Chen C, Chen C, Liu C, Xu MM, Zhao S, Shen B, Gao Y, Han D, He C. N (6)-methyladenosine of chromosome-associated regulatory RNA regulates chromatin state and transcription. Science. 2020;367:580–6.
11. Frye M, Harada BT, Behm M, He C. RNA modifications modulate gene expression during development. Science. 2018;361:1346–9.
12. Zeng L, Huang X, Zhang J, Lin D, Zheng J. Roles and implications of mRNA N(6) -methyladenosine in cancer. Cancer Commun (Lond). 2023;43:729–48.
13. Zou Y, Zheng S, Xie X, Ye F, Hu X, Tian Z, Yan SM, Yang L, Kong Y, Tang Y, et al. N6-methyladenosine regulated FGFR4 attenuates ferroptotic cell death in recalcitrant HER2-positive breast cancer. Nat Commun. 2022;13:2672.
14. Xu YY, Li T, Shen A, Bao XQ, Lin JF, Guo LZ, Meng Q, Ruan DY, Zhang QH, Zuo ZX, Zeng ZL. FTO up-regulation induced by MYC suppresses tumour progression in Epstein-Barr virus-associated gastric cancer. Clin Transl Med. 2023;13:e1505.
15. Hu Y, Gao Q, Ma S, Yu P, Ding S, Yao X, Zhang Z, Lu S, Lu M, Zhang J, et al. FMR1 promotes the progression of colorectal cancer cell by stabilizing EGFR mRNA in an m(6)A-dependent manner. Cell Death Dis. 2022;13:941.
16. Lu W, Yang X, Zhong W, Chen G, Guo X, Ye Q, Xu Y, Qi Z, Ye Y, Zhang J et al. METTL14-mediated m6A epitranscriptomic modification contributes to chemotherapy-induced neuropathic pain by stabilizing GluN2A expression via IGF2BP2. J Clin Invest 2024, 134.
17. Chang M, Wang Z, Gao J, Yang C, Feng M, Niu Y, Tong WM, Bao X, Wang R. METTL3-mediated RNA m6A hypermethylation promotes tumorigenesis and GH Secretion of Pituitary Somatotroph Adenomas. J Clin Endocrinol Metab. 2022;107:136–49.
18. Zhang W, Chen S, Du Q, Bian P, Chen Y, Liu Z, Zheng J, Sai K, Mou Y, Chen Z, et al. CircVPS13C promotes pituitary adenoma growth by decreasing the stability of IFITM1 mRNA via interacting with RRBP1. Oncogene. 2022;41:1550–62.
19. Du Q, Hu B, Feng Y, Wang Z, Wang X, Zhu D, Zhu Y, Jiang X, Wang H. circOMA1-Mediated mir-145-5p suppresses Tumor Growth of Nonfunctioning Pituitary Adenomas by Targeting TPT1. J Clin Endocrinol Metab. 2019;104:2419–34.
20. Chen S, Zhou Y, Chen Y, Gu J. Fastp: an ultra-fast all-in-one FASTQ preprocessor. Bioinformatics. 2018;34:i884–90.
21. Bao X, Zhu K, Liu X, Chen Z, Luo Z, Zhao Q, Ren J, Zuo Z. MeRIPseqPipe: an integrated analysis pipeline for MeRIP-seq data based on Nextflow. Bioinformatics. 2022;38:2054–6.
22. Dobin A, Davis CA, Schlesinger F, Drenkow J, Zaleski C, Jha S, Batut P, Chaisson M, Gingeras TR. STAR: ultrafast universal RNA-seq aligner. Bioinformatics. 2013;29:15–21.
23. Zhang Y, Liu T, Meyer CA, Eeckhoute J, Johnson DS, Bernstein BE, Nusbaum C, Myers RM, Brown M, Li W, Liu XS. Model-based analysis of ChIP-Seq (MACS). Genome Biol. 2008;9:R137.
24. Cui X, Meng J, Zhang S, Chen Y, Huang Y. A novel algorithm for calling mRNA m6A peaks by modeling biological variances in MeRIP-seq data. Bioinformatics. 2016;32:i378–85.
25. Quinlan AR, Hall IM. BEDTools: a flexible suite of utilities for comparing genomic features. Bioinformatics. 2010;26:841–2.
26. Liao Y, Smyth GK, Shi W. featureCounts: an efficient general purpose program for assigning sequence reads to genomic features. Bioinformatics. 2014;30:923–30.
27. Love MI, Huber W, Anders S. Moderated estimation of Fold change and dispersion for RNA-seq data with DESeq2. Genome Biol. 2014;15:550.
28. Heinz S, Benner C, Spann N, Bertolino E, Lin YC, Laslo P, Cheng JX, Murre C, Singh H, Glass CK. Simple combinations of lineage-determining transcription factors prime cis-regulatory elements required for macrophage and B cell identities. Mol Cell. 2010;38:576–89.
29. Zhang Q, Yao B, Long X, Chen Z, He M, Wu Y, Qiao N, Ma Z, Ye Z, Zhang Y, et al. Single-cell sequencing identifies differentiation-related markers for molecular classification and recurrence prediction of PitNET. Cell Rep Med. 2023;4:100934.
30. Cui R, Duan H, Hu W, Li C, Zhong S, Liang L, Chen S, Hu H, He Z, Wang Z et al. Establishment of human pituitary neuroendocrine tumor derived Organoid and its pilot application for drug screening. J Clin Endocrinol Metab 2024.
31. Meyer KD, Saletore Y, Zumbo P, Elemento O, Mason CE, Jaffrey SR. Comprehensive analysis of mRNA methylation reveals enrichment in 3' UTRs and near stop codons. Cell. 2012;149:1635–46.
32. Asmaro K, Zhang M, Rodrigues AJ, Mohyeldin A, Vigo V, Nernekli K, Vogel H, Born DE, Katznelson L, Fernandez-Miranda JC. Cytodifferentiation of pituitary tumors influences pathogenesis and cavernous sinus invasion. J Neurosurg. 2023;139:1216–24.
33. Sokol E. Structure of Desmosomes. In *Autoimmune Bullous Diseases: Text and Review.* Edited by Horváth B. Cham: Springer International Publishing; 2022: 61–64.
34. Zhou Y, Zeng P, Li YH, Zhang Z, Cui Q. SRAMP: prediction of mammalian N6-methyladenosine (m6A) sites based on sequence-derived features. Nucleic Acids Res. 2016;44:e91.
35. Luo X, Li H, Liang J, Zhao Q, Xie Y, Ren J, Zuo Z. RMVar: an updated database of functional variants involved in RNA modifications. Nucleic Acids Res. 2021;49:D1405–12.
36. Zheng Y, Nie P, Peng D, He Z, Liu M, Xie Y, Miao Y, Zuo Z, Ren J. m6AVar: a database of functional variants involved in m6A modification. Nucleic Acids Res. 2018;46:D139–45.
37. Richter JD, Zhao X. The molecular biology of FMRP: new insights into fragile X syndrome. Nat Rev Neurosci. 2021;22:209–22.
38. Xiong W, Knox AJ, Xu M, Kiseljak-Vassiliades K, Colgan SP, Brodsky KS, Kleinschmidt-Demasters BK, Lillehei KO, Wierman ME. Mammalian Ste20-like kinase 4 promotes pituitary cell proliferation and survival under hypoxia. Mol Endocrinol. 2015;29:460–72.
39. Kristof RA, Aliashkevich AF, Hans V, Haun D, Meyer B, Thees C, Schramm J. The regional oxygen saturation of pituitary adenomas is lower than that of the pituitary gland: microspectrophotometric study with potential clinical implications. Neurosurgery. 2003;53:880–5. discussion 885–886.
40. Vidal S, Scheithauer BW, Kovacs K. Vascularity in Nontumorous Human pituitaries and Incidental Microadenomas: a morphometric study. Endocr Pathol. 2000;11:215–27.
41. Vidal S, Horvath E, Kovacs K, Kuroki T, Lloyd RV, Scheithauer BW. Expression of hypoxia-inducible factor-1alpha (HIF-1alpha) in pituitary tumours. Histol Histopathol. 2003;18:679–86.
42. Shimon I, Yan X, Taylor JE, Weiss MH, Culler MD, Melmed S. Somatostatin receptor (SSTR) subtype-selective analogues differentially suppress in vitro growth hormone and prolactin in human pituitary adenomas. Novel potential therapy for functional pituitary tumors. J Clin Invest. 1997;100:2386–92.
43. Tuggle CK, Trenkle A. Control of growth hormone synthesis. Domest Anim Endocrinol. 1996;13:1–33.
44. Bertherat J. Nuclear effects of the cAMP pathway activation in somatotrophs. Horm Res. 1997;47:245–50.
45. Mayo KE, Godfrey PA, Suhr ST, Kulik DJ, Rahal JO. Growth hormone-releasing hormone: synthesis and signaling. Recent Prog Horm Res. 1995;50:35–73.
46. Spada A, Arosio M, Bochicchio D, Bazzoni N, Vallar L, Bassetti M, Faglia G. Clinical, biochemical, and morphological correlates in patients bearing growth hormone-secreting pituitary tumors with or without constitutively active adenylyl cyclase. J Clin Endocrinol Metab. 1990;71:1421–6.
47. Bakhtiar Y, Hirano H, Arita K, Yunoue S, Fujio S, Tominaga A, Sakoguchi T, Sugiyama K, Kurisu K, Yasufuku-Takano J, Takano K. Relationship between cytokeratin staining patterns and clinico-pathological features in somatotropinomae. Eur J Endocrinol. 2010;163:531–9.

48. Fougner SL, Casar-Borota O, Heck A, Berg JP, Bollerslev J. Adenoma granulation pattern correlates with clinical variables and effect of somatostatin analogue treatment in a large series of patients with acromegaly. Clin Endocrinol (Oxf). 2012;76:96–102.
49. Larkin S, Reddy R, Karavitaki N, Cudlip S, Wass J, Ansorge O. Granulation pattern, but not GSP or GHR mutation, is associated with clinical characteristics in somatostatin-naive patients with somatotroph adenomas. Eur J Endocrinol. 2013;168:491–9.
50. Landis CA, Masters SB, Spada A, Pace AM, Bourne HR, Vallar L. GTPase inhibiting mutations activate the alpha chain of gs and stimulate adenylyl cyclase in human pituitary tumours. Nature. 1989;340:692–6.
51. Adams EF, Brockmeier S, Friedmann E, Roth M, Buchfelder M, Fahlbusch R. Clinical and biochemical characteristics of acromegalic patients harboring gsp-positive and gsp-negative pituitary tumors. Neurosurgery. 1993;33:198–203. discussion 203.
52. Asa SL, Digiovanni R, Jiang J, Ward ML, Loesch K, Yamada S, Sano T, Yoshimoto K, Frank SJ, Ezzat S. A growth hormone receptor mutation impairs growth hormone autofeedback signaling in pituitary tumors. Cancer Res. 2007;67:7505–11.
53. Kola B, Korbonits M, Diaz-Cano S, Kaltsas G, Morris DG, Jordan S, Metherell L, Powell M, Czirjak S, Arnaldi G, et al. Reduced expression of the growth hormone and type 1 insulin-like growth factor receptors in human somatotroph tumours and an analysis of possible mutations of the growth hormone receptor. Clin Endocrinol (Oxf). 2003;59:328–38.
54. Di Bella G, Colori B, Scanferlato R. The over-expression of GH/GHR in tumour tissues with respect to healthy ones confirms its oncogenic role and the consequent oncosuppressor role of its physiological inhibitor, somatostatin: a review of the literature. Neuro Endocrinol Lett. 2018;39:179–88.
55. Kopchick JJ, Basu R, Berryman DE, Jorgensen JOL, Johannsson G, Puri V. Covert actions of growth hormone: fibrosis, cardiovascular diseases and cancer. Nat Rev Endocrinol. 2022;18:558–73.
56. Clayton PE, Banerjee I, Murray PG, Renehan AG. Growth hormone, the insulin-like growth factor axis, insulin and cancer risk. Nat Rev Endocrinol. 2011;7:11–24.
57. Boguszewski CL, Boguszewski M. Growth hormone's links to Cancer. Endocr Rev. 2019;40:558–74.

Publisher's note